Journal of Pathology
J Pathol 2019; **247:** 357–370
Published online 16 January 2019 in Wiley Online Library (wileyonlinelibrary.com) DOI: 10.1002/path.5195

ORIGINAL PAPER

Long non-coding RNAs influence the transcriptome in pulmonary arterial hypertension: the role of *PAXIP1-AS1*

Katharina Jandl[1†], Helene Thekkekara Puthenparampil[1†], Leigh M Marsh[1], Julia Hoffmann[1], Jochen Wilhelm[2], Christine Veith[3], Katharina Sinn[4], Walter Klepetko[4], Horst Olschewski[1,5], Andrea Olschewski[1,6], Matthias Brock[7] and Grazyna Kwapiszewska[1,6*]

[1] *Ludwig Boltzmann Institute for Lung Vascular Research, Graz, Austria*
[2] *Department of Internal Medicine, Justus-Liebig-University Giessen, Universities of Giessen and Marburg Lung Center, German Center for Lung Research, Giessen, Germany*
[3] *Excellence Cluster Cardio-Pulmonary System, Justus-Liebig-University Giessen, Universities of Giessen and Marburg Lung Center, German Center for Lung Lung Research, Giessen, Germany*
[4] *Division of Thoracic Surgery, Department of Surgery, Medical University of Vienna, Vienna, Austria*
[5] *Division of Pulmonology, Department of Internal Medicine, Medical University of Graz, Graz, Austria*
[6] *Otto Loewi Research Center, Chair of Physiology, Medical University of Graz, Graz, Austria*
[7] *Division of Pulmonology, University Hospital Zürich, University of Zürich, Zürich, Switzerland*

**Correspondence to: G Kwapiszewska, Ludwig Boltzmann Institute for Lung Vascular Research, c/o ZMF, Stiftingtalstrasse 24, 8010 Graz, Austria. E-mail: grazyna.kwapiszewska@lvr.lbg.ac.at*

[†]These authors contributed equally to this work.

Abstract

In idiopathic pulmonary arterial hypertension (IPAH), global transcriptional changes induce a smooth muscle cell phenotype characterised by excessive proliferation, migration, and apoptosis resistance. Long non-coding RNAs (lncRNAs) are key regulators of cellular function. Using a compartment-specific transcriptional profiling approach, we sought to investigate the link between transcriptional reprogramming by lncRNAs and the maladaptive smooth muscle cell phenotype in IPAH. Transcriptional profiling of small remodelled arteries from 18 IPAH patients and 17 controls revealed global perturbations in metabolic, neuronal, proliferative, and immunological processes. We demonstrated an IPAH-specific lncRNA expression profile and identified the lncRNA *PAXIP1-AS1* as highly abundant. Comparative transcriptomic analysis and functional assays revealed an intrinsic role for *PAXIP1-AS1* in orchestrating the hyperproliferative and migratory actions of IPAH smooth muscle cells. Further, we showed that *PAXIP1-AS1* mechanistically interferes with the focal adhesion axis via regulation of expression and phosphorylation of its downstream target paxillin. Overall, we show that changes in the lncRNA transcriptome contribute to the disease-specific transcriptional landscape in IPAH. Our results suggest that lncRNAs, such as *PAXIP1-AS1*, can modulate smooth muscle cell function by affecting multiple IPAH-specific transcriptional programmes.

Keywords: lncRNA; vascular diseases; paxillin; pulmonary hypertension; vascular remodelling; pulmonary artery smooth muscle cells

Received 15 May 2018; Revised 18 September 2018; Accepted 2 November 2018

No conflicts of interest were declared.

The copyright line for this article was changed on 13 November 2019 after original online publication.

Introduction

Pulmonary arterial hypertension (PAH) is a severe and progressive disease which ultimately leads to right heart failure [1]. Within the vessel wall, multiple factors contribute to the increased pulmonary pressure, including cellular hyperplasia and extracellular matrix (ECM) deposition [2,3]. In the medial layer, smooth muscle cells (SMCs) show increased proliferation [4], invasive migratory capacity, and resistance to apoptosis [5]. These functional alterations are accompanied by a reprogramming of cellular respiration [6] and glucose expenditure [7]. PAH has a strong genetic predisposition, with several mutations contributing to the disease development [8]. Loss-of-function mutations in *BMPR2* occur in over 70% of patients with familial PAH and in 25% of patients with the idiopathic form [9]. However, *BMPR2* mutations show only 20% penetrance [10]. Thus, it is apparent that additional regulatory mechanisms are involved and factors other than solely mutations in coding genes are required for disease development.

The human genome contains approximately equal numbers of coding and non-coding genes (GENCODE Release, version 29). Despite being highly abundant, non-coding genes are still under-studied. The

non-coding transcriptome includes many regulatory transcripts, which can be roughly classified into small non-coding RNAs (sncRNAs, < 200 nt), including the group of microRNAs (miRNAs), and long non-coding RNAs (lncRNAs, > 200 nt) [11]. Variations in disease complexity and penetrance of genetic variants are increasingly attributed to changes in gene expression of the non-coding genome, rather than to changes within protein-coding sequences [12].

In contrast to sncRNAs, which act via RNA binding, lncRNAs exert their regulatory effects, both at the transcriptional and at the post-transcriptional levels, via interactions with DNA, chromatin, and other RNA species [13]. In addition, lncRNAs can bind chromatin-modifying proteins such as histone modifiers, and thus act as epigenetic modulators [14,15]. In this respect, lncRNAs often regulate fundamental cellular processes, such as proliferation or apoptosis [16,17]. Due to the tight transcriptional regulation of lncRNAs and their specific subcellular localisation, a 'long non-coding' landscape can be generated, which is highly cell-type, tissue, and disease-specific [11,18,19].

In the field of pulmonary vascular remodelling, sncRNAs such as miRNAs have been intensively studied and constitute well-recognised cellular control mechanisms [20–24]. In contrast, lncRNAs are under-investigated in this field. In the present study, we have characterised the gene expression profiles of coding and non-coding genes from small pulmonary arteries obtained via laser-capture microdissection (LCM) from IPAH and control lungs. We focus on the functional role of a highly deregulated lncRNA, *PAXIP1-AS1*, in perpetuating the migratory and proliferative phenotype of IPAH pulmonary artery smooth muscle cells (PASMCs).

Materials and methods

Genome-wide expression profiling

Briefly, whole genome expression profiling was performed on material obtained from small pulmonary arteries (50–500 µm in diameter, consisting of intima and media) isolated using LCM from IPAH patients and down-sized non-tumorous, non-transplanted donor lungs [approved by the institutional ethics committee (976/2010)]. The patients' key clinical characteristics are listed in Table 1. A detailed description of the procedure is provided in the supplementary material, Supplementary materials and methods.

Bioinformatic analysis

Several online tools (RegRNA 2.0, CPC, CPAT, Vienna RNA Websuite, BLAST, NetworkAnalyst) [25–32] were used to explore the RNA sequence and the obtained expression profiling data.

Table 1. Clinical characteristics of the donors and IPAH patients in this study

	Donors ($n = 17$)	IPAH ($n = 18$)	*P* value
Age, years	46 ± 12	32 ± 12	0.0016
Sex, M/F	8/9	4/14	0.1218
HR, beats/min		87.8 ± 9.7	
mPAP, mmHg		76.3 ± 22.1	
PAWP, mmHg		10.6 ± 4	
RA, mmHg			
CO, l/min		3.5 ± 1.6	
CI, l/min/m^2		2.1 ± 0.9	
PO_2, mmHg		66.2 ± 19.3	
PCO_2, mmHg		31 ± 6.1	
PVR, dyn·s/cm^5		1665.4 ± 799.7	
6MWD, m		298.7 ± 188.2	
NT-proBNP, pg/ml		4061.9 ± 2578	
CRP, mg/l		0.56 ± 0.5	
Bilirubin, mg/dl		1.8 ± 2.1	
Uric acid, mg/dl		7 ± 1.7	

6MWD, 6-min walking distance; CI, cardiac index; CO, cardiac output; CRP, C-reactive protein; F, female; HR, heart rate; IPAH, idiopathic pulmonary arterial hypertension; M, male; mPAP, mean pulmonary arterial pressure; NT-proBNP, NH_2-terminal pro-brain natriuretic peptide; PAWP, pulmonary arterial wedge pressure; PCO_2, partial pressure of carbon dioxide; PO_2, partial pressure of oxygen; PVR, pulmonary vascular resistance; RA, right atrial pressure.

Cell culture, transfection, and functional assays

Human PASMCs were bought (Lonza, Basel, Switzerland) or isolated from pulmonary arteries from non-transplanted donor lungs or IPAH lungs. siRNA- and GapmeR-mediated knockdown was performed 48 h before performing the functional experiments, details of which are given in the supplementary material, Supplementary materials and methods.

Immunofluorescence staining and western blot analysis

For immunostaining, PASMCs were seeded on eight-well chamber slides and fixed in 4% paraformaldehyde 48 h after transfection. For protein extraction, PASMCs were transfected with GapmeRs or siRNAs, respectively, and whole cell lysates were prepared using 2× Laemmli sample buffer 48 h after transfection. The antibodies used and further details of the procedures are given in the supplementary material, Supplementary materials and methods.

Subcellular fractionation

RNA for the subcellular fractioning was obtained from PASMCs seeded at a density of 8×10^3 cells/cm^2 and allowed to grow to 80% confluency in 10-mm Petri dishes. The precipitation and subsequent purification of the RNA were performed as described elsewhere [33].

Gene expression analysis

Details of RNA isolation, cDNA synthesis, and quantitative real-time PCR (qRT-PCR) analysis are given in the supplementary material, Supplementary materials and methods.

Fluorescence *in situ* hybridisation

In situ hybridisation analysis of *PAXIP1-AS1* in PASMCs and frozen lung sections (5 µm) was performed using the ViewRNA® Cell Plus Assay (Thermo Fisher Scientific, Waltham, MA, USA). Details may be found in the supplementary material, Supplementary materials and methods.

Statistics

Mean differences were tested using the two-sided independent-sample or paired-sample *t*-test. The tests were performed on the logarithms of the concentrations and on the logits of proportions. One-way analysis of variance (ANOVA) with Tukey's HSD was used to correct for multiple testing. A chi-square test of independence was performed in case of categorical variables. Values of $p < 0.05$ were considered statistically significant. The n number indicates independent experiments. Graphs and statistical calculations were performed using the software package GraphPad Prism Version 5.0 (GraphPad Software, San Diego, CA, USA, RStudio (https://www.rstudio.com) or R (https://www.r-project.org).

Additional information on methods and reagents is available in the supplementary material, Supplementary materials and methods.

Results

IPAH small remodelled arteries possess a distinct coding and long non-coding transcriptional profile

One hallmark of PAH is the remodelling of small distal pulmonary arteries [34]. We defined the gene expression profile in small pulmonary arteries of 18 IPAH patients and 17 controls. Based on a minimum significance ($-\log_{10} p$) of 3 and a minimum absolute $\log_2$ fold change (LFC) of 1.25, 124 annotated protein-coding genes were classified as up- (76) or down-regulated (48) in IPAH compared with control donor samples (Figure 1A and supplementary material, Table S1). A KEGG pathway analysis following gene set enrichment on the entire dataset indicated a perturbation in metabolic, immunological, neuronal, and proliferative processes in IPAH (Figure 1B and supplementary material, Figure S1A). Connections between regulated genes of the top ten perturbed KEGG pathways are displayed in the supplementary material, Figure S1B. The individual profiles of the 50 genes with the highest significance are shown in the heatmap in Figure 1C. Gene ontology assigned these genes to several nodes, which were overrepresented in IPAH; these predominantly belonged to the groups of phospholipid and nitrogen metabolism, proliferation, immunological and neuronal responses, signal transduction (involving tyrosine receptor kinases and small GTPases), and transcriptional regulation (Figure 1D). In addition to protein-coding genes, we identified a large number of differentially regulated non-coding RNAs. This heterogeneous group included long intergenic non-coding (linc) RNAs, antisense (as) RNAs, pseudogenes, and other long and small ncRNAs, as depicted in Figure 1E. By excluding non-annotated transcripts and transcripts shorter than 200 nt, we identified a total of 146 regulated non-coding genes (supplementary material, Table S2). Changes in the expression of non-coding RNA genes thus contribute substantially to the unique transcriptomic landscape of IPAH vessels (Figure 1F). The lncRNA profiles of IPAH and donor groups were clearly distinct (Figure 1G). The differential expression of seven of the ten most regulated lncRNAs (Figure 1H) was analysed by qRT-PCR. The lncRNAs *TUSC8* and *PAXIP1-AS1* were verified to be upregulated in IPAH (Figure 1I). As *PAXIP1-AS1* was previously reported to be involved in proliferative events [35], we selected it for further analysis. Following a t-stochastic neighbouring embedding (t-SNE) dimension reduction of all detected genes, *PAXIP1-AS1* expression levels at single patient level were visualised in a colour-by-expression code. Indeed, the heatmap overlay of *PAXIP1-AS1* expression resembles the clear discrimination of IPAH and donor transcriptome in the t-SNE plot (Figure 1J).

PAXIP1-AS1 expression is enhanced in human IPAH-PASMCs and knockdown reveals its involvement in focal adhesion and ECM–receptor interaction

PAXIP1-AS1 comprises a single exon located at chromosome 7q36.2 (position: 155003433–155005703; NC_000007.14, GRCh38.p12 according to the NCBI database). It is flanked on its 5′ side by a GC-rich region that separates it from its diverging coding gene *PAXIP1* on the opposite strand. To identify whether *PAXIP1-AS1* expression is limited to the lung, we explored its expression across multiple human tissues using the Genotype-Tissue Expression (GTEx) portal. Low ubiquitous expression was observed in multiple tissues, with a notable enrichment in the cerebellum (supplementary material, Figure S2A,B). Closer examination of *PAXIP1-AS1* expression by qRT-PCR revealed that *PAXIP1-AS1* was enriched in pulmonary arteries without adventitia, compared with pulmonary veins, bronchi, and pulmonary arterial adventitia (supplementary material, Figure S2C). Furthermore, in isolated cells, *PAXIP1-AS1* expression was highest in parenchymal fibroblasts and PASMCs, followed by adventitial fibroblasts and pulmonary arterial endothelial cells (supplementary material, Figure S2D).

Although *PAXIP1-AS1* harbours a putative open-reading frame, online coding potential calculators suggested only a weak coding potential (supplementary material, Figure S3A,B and Figure 2A). *PAXIP1-AS1* structure prediction resulted in a complex alignment and its high stability given by the calculated free energy suggests a functional importance (Figure 2B). We therefore investigated the transcript for functional sequences

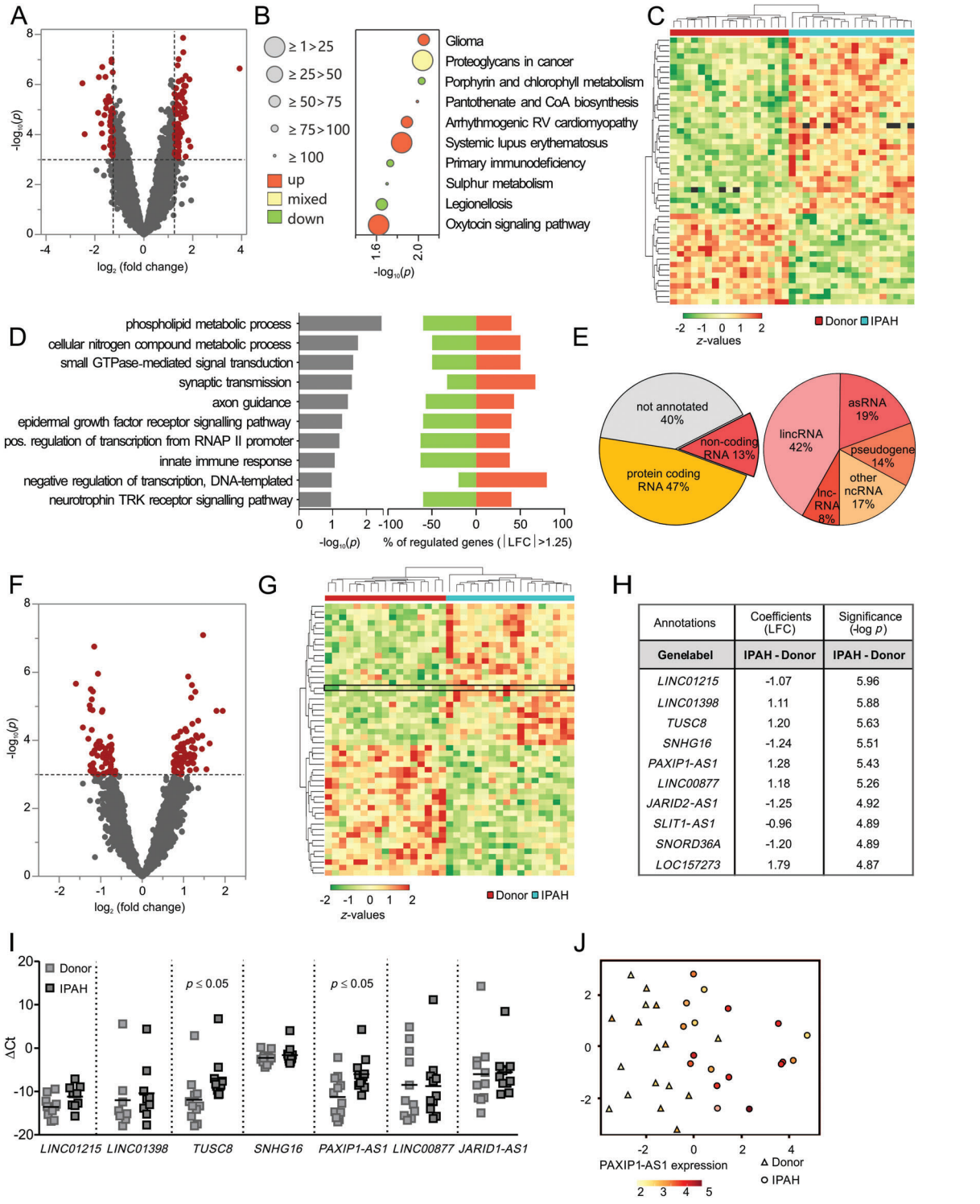

Annotations	Coefficients (LFC)	Significance (-log *p*)
Genelabel	**IPAH - Donor**	**IPAH - Donor**
LINC01215	-1.07	5.96
LINC01398	1.11	5.88
TUSC8	1.20	5.63
SNHG16	-1.24	5.51
PAXIP1-AS1	1.28	5.43
LINC00877	1.18	5.26
JARID2-AS1	-1.25	4.92
SLIT1-AS1	-0.96	4.89
SNORD36A	-1.20	4.89
LOC157273	1.79	4.87

Figure 1. Expression profiling of small pulmonary arteries from IPAH and control donors reveals dysregulation of metabolic, proliferative, and immune-neuronal pathways and the lncRNA transcriptome. (A) Volcano plot of differentially expressed genes in small pulmonary arteries of IPAH patients. (B) Top ten KEGG pathways after gene set enrichment from all detected genes. (C) Heatmap representing the expression distribution at single patient levels of the 50 most regulated genes. (D) Top ten GO terms (biological processes) after overrepresentation analysis, defined by a minimum significance ($-\log_{10}$ *p*) of 3 and a minimum absolute LFC of 1.25. Left, $-\log_{10}$ *p* of the perturbation determined from a gene set test; right, percentage of genes from corresponding GO nodes that are up- and down-regulated. (E) Pie-charts depicting the proportion of protein-coding and non-protein-coding genes, and the categorisation of the non-coding RNA genes identified in the transcriptome analysis. (F) Volcano plot showing differentially regulated ncRNAs as determined by a minimum $-\log_{10}$ *p* of 3. (G) Heatmap representing the expression levels of the 50 most regulated lncRNAs at single patient level. *PAXIP1-AS1* is highlighted. (H) Annotation and regulation parameters of the top ten regulated lncRNAs in small pulmonary arteries of IPAH patients. (I) qPCR validation of transcriptome analysis. (J) Single patient t-distributed stochastic neighbour embedding (t-SNE) analysis showing the distance between single samples with colour-by-expression coding of *PAXIP1-AS1* and respective annotation according to disease.

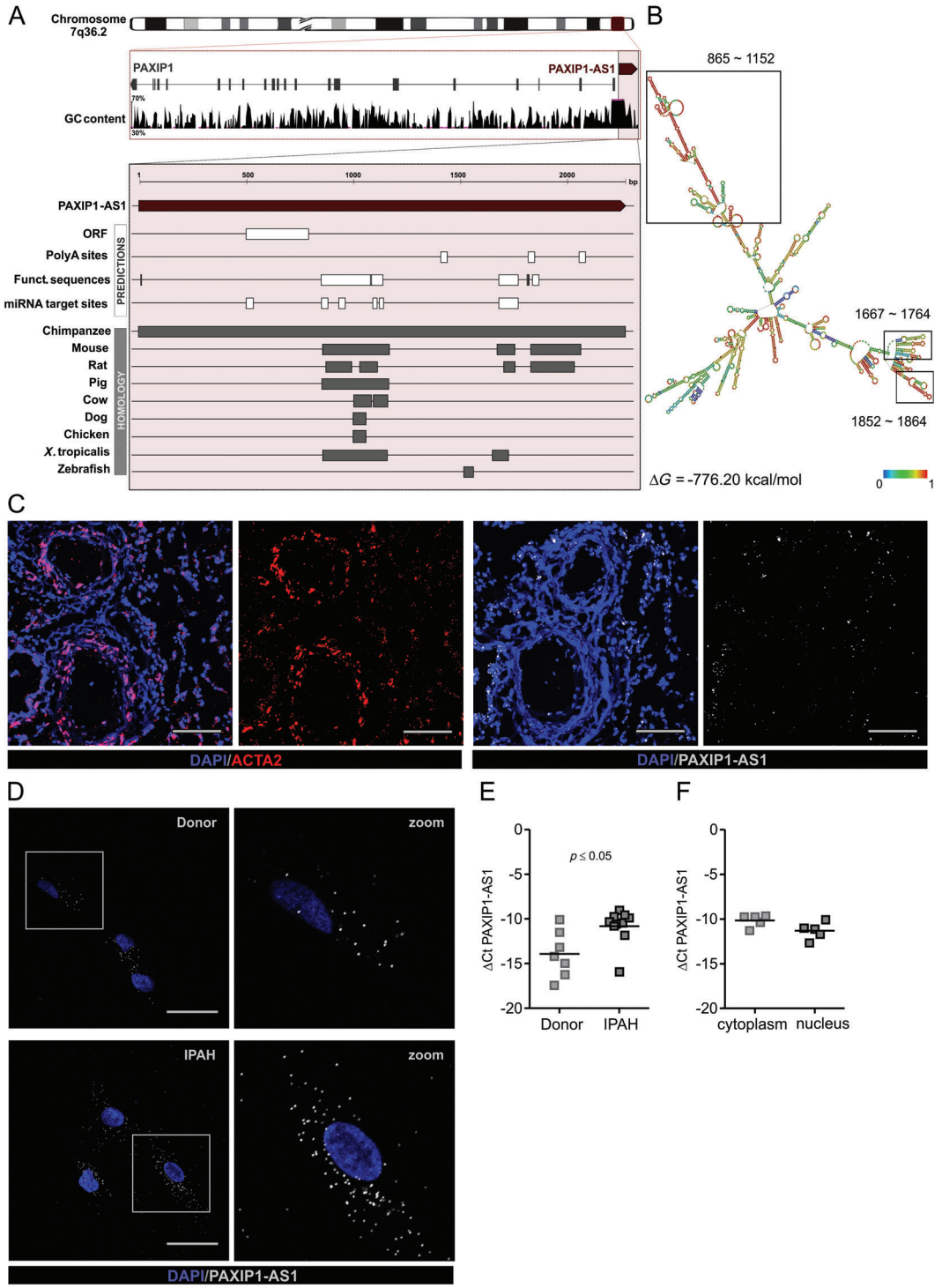

Figure 2. *PAXIP1-AS1* harbours functional sequences and is abundantly expressed in IPAH-PASMCs. (A) Chromosomal location and sequence characteristics of *PAXIP1-AS1* (adapted from entry in UCSC Genome Browser on Human, December 2013 (GRCh38/hg38) Assembly; UCSC ID: uc010lqi.6). Predicted features (white bars) for the transcript of *PAXIP1-AS1* and conserved regions (grey bars) in exemplary organisms are depicted. Note the occurrence of Alu- and AU-rich elements, and their positional concordance to the conserved regions in various species (see supplementary material, Table S3 for detailed positioning). (B) Predicted secondary structure of lncRNA *PAXIP1-AS1* calculated using the partition function and base-pairing probability matrix in addition to the minimum free energy (MFE) structure. The most optimal structure ($\Delta G = -776.20$ kcal/mol) is depicted; the approximate Alu- and AU-rich regions are highlighted. Colour intensity denotes base-pairing probabilities (red = most likely; colour at unpaired regions denotes probability of being unpaired). (C) Representative RNA fluorescence *in situ* hybridisation images of *ACTA1* in red and *PAXIP1-AS1* in grey on serial cryo sections (5 µm) of IPAH lungs ($n = 2$). Scale bar = 100 µm. (D) Fluorescent images of *PAXIP1-AS1* (red) RNA *in situ* hybridisation on PASMCs of IPAH and donors ($n = 2$). Scale bar = 50 µm. qRT-PCR of *PAXIP1-AS1* in PASMCs of IPAH and donors (E) and after subcellular fractionation of PASMCs (F). $p \leq 0.05$ as determined by Student's *t*-test.

to further delineate possible biological functions. Several Alu elements, SRP RNA, A- and C-repeats, and an AU-rich element were identified (Figure 2A and supplementary material, Table S3). Furthermore, the predictions suggest several binding sites for miRNA as well as transcription factors (supplementary material, Tables S4 and S5). Like most lncRNAs [36], *PAXIP1-AS1* lacks conservation across species beyond primates.

To identify which cells in the pulmonary artery are responsible for increased *PAXIP1-AS1* levels, we visualised its expression in human IPAH tissue using fluorescence *in situ* hybridisation (FISH). *PAXIP1-AS1* was expressed in the lung with abundance in α-smooth muscle actin-expressing cells (Figure 2C and supplementary material, Figure S4A). The expression of *PAXIP1-AS1* was further validated in PASMCs isolated from donors and IPAH (Figure 2D,E and supplementary material, Figure S4B). Interestingly, a similar increase was also observed in adventitial, but not parenchymal, IPAH fibroblasts (supplementary material, Figure S2E).

The subcellular localisation of lncRNAs is critical for determining their functional properties. Both FISH and subcellular fractionation experiments detected *PAXIP1-AS1* in both the nuclear and the cytoplasmic compartments (Figure 2D,F). Next, we checked whether *PAXIP1-AS1* transcription can be modulated by mediators that are involved in PAH pathogenesis. Treatment of PASMCs with endothelin-1 (ET-1) suggested a susceptibility of *PAXIP1-AS1* expression to the endothelial-derived mediator (supplementary material, Figure S5).

To delineate how *PAXIP1-AS1* can influence PASMC function, we analysed the gene expression profile following GapmeR-mediated *PAXIP1-AS1* knockdown. A clear change in the transcriptional programme was observed, as highlighted by the volcano plot (Figure 3A and supplementary material, Table S6) and in the heatmap representation of the top 100 regulated genes (Figure 3B). Notably, the profiles of untransfected samples were nearly identical to scrambled control-treated samples (Figure 3B). To gain insights into the global changes induced after *PAXIP1-AS1* knockdown in PASMCs, we performed a KEGG pathway analysis of all regulated transcripts. *PAXIP1-AS1* silencing perturbed protein turnover, cytoskeletal arrangement at focal adhesions, extracellular matrix, and pathways implicated in metabolic and proliferative processes (Figure 3C). The genes involved in these pathways are shown in Figure 3D and supplementary material, Table S7. Importantly, *PXN*, encoding the focal adhesion adaptor protein paxillin, was one of the top ten regulated genes in two different KEGG pathways (highlighted in Figure 3D). To delineate how *PAXIP1-AS1* could exert its effects in IPAH, we investigated potential downstream effectors in IPAH arteries. To this end, we directly compared genes classified as differentially expressed from our two transcriptomic profiling approaches: (1) LCM arteries from IPAH versus donor, and (2) PASMCs after *PAXIP1-AS1* knockdown. This comparison revealed 61 genes as regulated in common in both approaches (Figure 3E and supplementary material, Table S8). Next, we narrowed the number of genes to 32 by selecting only genes that were regulated in opposite directions, thereby identifying a potential *PAXIP1-AS1*-regulated gene set in IPAH. Amongst those, several were implicated in proliferation and apoptosis processes, e.g. the cyclin G-associated kinase (*GAK*) and cullin 1 (*CUL1*) (Figure 3F).

PAXIP1-AS1 inhibition promoted apoptosis and inhibited PASMC proliferation and migration via its downstream target paxillin

To substantiate the involvement of *PAXIP1-AS1* in proliferation and apoptosis, we used two complementary loss-of-function approaches, GapmeR and siRNA-mediated knockdown (Figure 4A). Indeed, forced reduction of *PAXIP1-AS1* potently reduced proliferation and elevated pro-apoptotic events in PASMCs (Figure 4B,C). As focal adhesions and ECM–receptor interaction pathways were perturbed after *PAXIP1-AS1* knockdown, we also investigated its role in migratory processes. As observed in a scratch wound healing assay, both knockdown approaches of *PAXIP1-AS1* resulted in a marked reduction in the migratory potential of PASMCs (Figure 4D,E).

The *PAXIP1-AS1*–paxillin axis contributes to the IPAH PASMC phenotype

Changes in focal adhesions can contribute to disease progression. To delineate the intrinsic mechanism of *PAXIP1-AS1* on changes in focal adhesions, we focused on paxillin as a downstream effector of *PAXIP1-AS1* in healthy donor PASMCs. We confirmed that depletion of *PAXIP1-AS1* resulted in decreased total and phospho (p)-paxillin protein levels (Figure 5A,B). Since precise coordination between focal adhesions and the actin cytoskeleton is essential for cell migration, we visualised p-paxillin together with F-actin on donor PASMCs. After *PAXIP1-AS1* knockdown, p-paxillin levels were decreased, whereas F-actin levels increased (Figure 5C,D). Plotting of the cross-sectional F-actin signal suggested cytoskeletal rearrangement and increased stress fibre formation visualised in the number and width of peaks in response to the knockdown of *PAXIP1-AS1* (Figure 5E and supplementary material, Figure S6A,B). This suggests that knockdown of *PAXIP1-AS1* and the reduced levels of paxillin trigger a stress response in the cells. Interestingly, the focal adhesion kinase (FAK), another focal adhesion protein, showed a similar tendency to downregulation after knockdown of *PAXIP1-AS1* (supplementary material, Figure S7A–C). Next, we translated these findings into the patient context, and investigated paxillin in IPAH PASMCs. We detected increased total and p-paxillin protein levels, but no robust changes in mRNA expression in IPAH PASMCs compared with donors (Figure 5F,G and supplementary

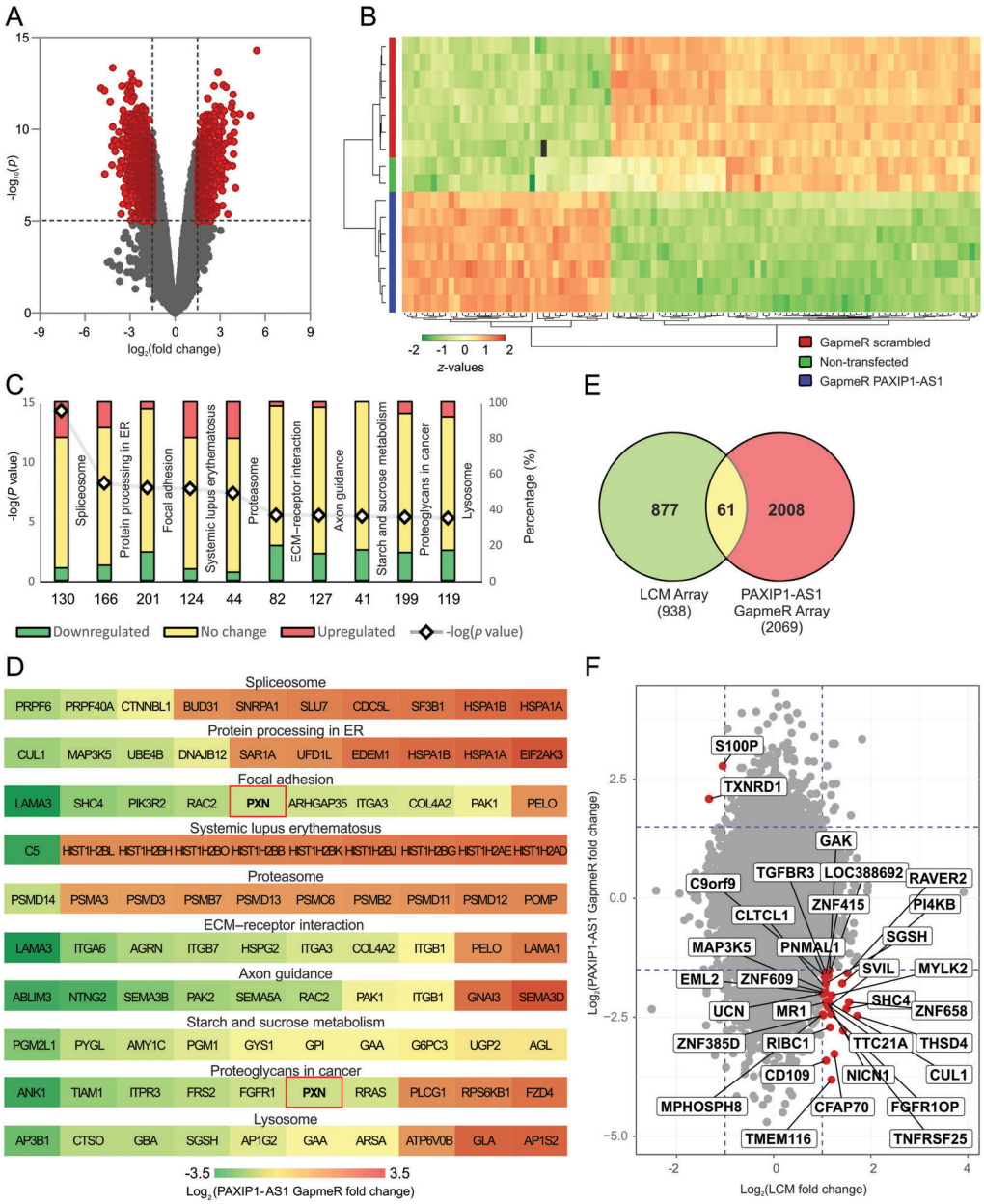

Figure 3. Genes and gene sets dependent on *PAXIP1-AS1* in IPAH. (A) Volcano plot of $\log_2$ ratio highlighting differentially expressed genes applying a cut-off of a minimum $-\log_{10}$ *p* of 5 and a minimum absolute LFC of 1.5 after forced knockdown of *PAXIP1-AS1* on PASMCs. (B) Heatmap representing the top 100 regulated genes. (C) KEGG-pathway analysis of gene set enrichment of all genes in PASMCs after knockdown of *PAXIP1-AS1*.–$\log_{10}$ *P* values of the perturbation and the percentages of genes from corresponding KEGG pathway that are down- and up-regulated are depicted. (D) Heatmap of the LFC of the ten most regulated genes from the top ten perturbed pathways (as in C). (E) Overlapping regulated genes of transcriptome analysis of arteries obtained by LCM from donor and IPAH and transcriptome analysis after *PAXIP1-AS1* knockdown in PASMCs. (F) Comparison as in E highlighting inversely regulated genes.

material, Figure S8A). In IPAH PASMCs, the increased levels of p-paxillin were accompanied by an increase in F-actin levels and appeared locally associated with both ventral and distal stress fibres (Figure 5H–J, and supplementary material, Figure S6C,D). Collectively, this suggested a link between the lncRNA *PAXIP1-AS1* and IPAH PASMC function that depends on the cytoskeleton and the focal adhesion protein paxillin.

To further examine this link, we next performed *PAXIP1-AS1* knockdown experiments in IPAH PASMCs. Here, *PAXIP1-AS1* knockdown robustly reduced total paxillin protein levels, while F-actin levels were unaffected (Figure 6A–C). Knockdown of *PAXIP1-AS1* in IPAH PASMCs led to increased apoptotic susceptibility, which was rescued by simultaneous overexpression of paxillin (Figure 6D,E and supplementary material, Figure S8B,C). While knockdown of *PAXIP1-AS1* robustly decreased total protein paxillin levels, we could not observe consistent changes in the gene expression levels of paxillin (supplementary material, Figure S8C). Next, we overexpressed *PAXIP1-AS1* in both donor and IPAH PASMCs (Figure 6F) and investigated its effect on apoptosis resistance. Overexpression of the lncRNA *PAXIP1-AS1* potently

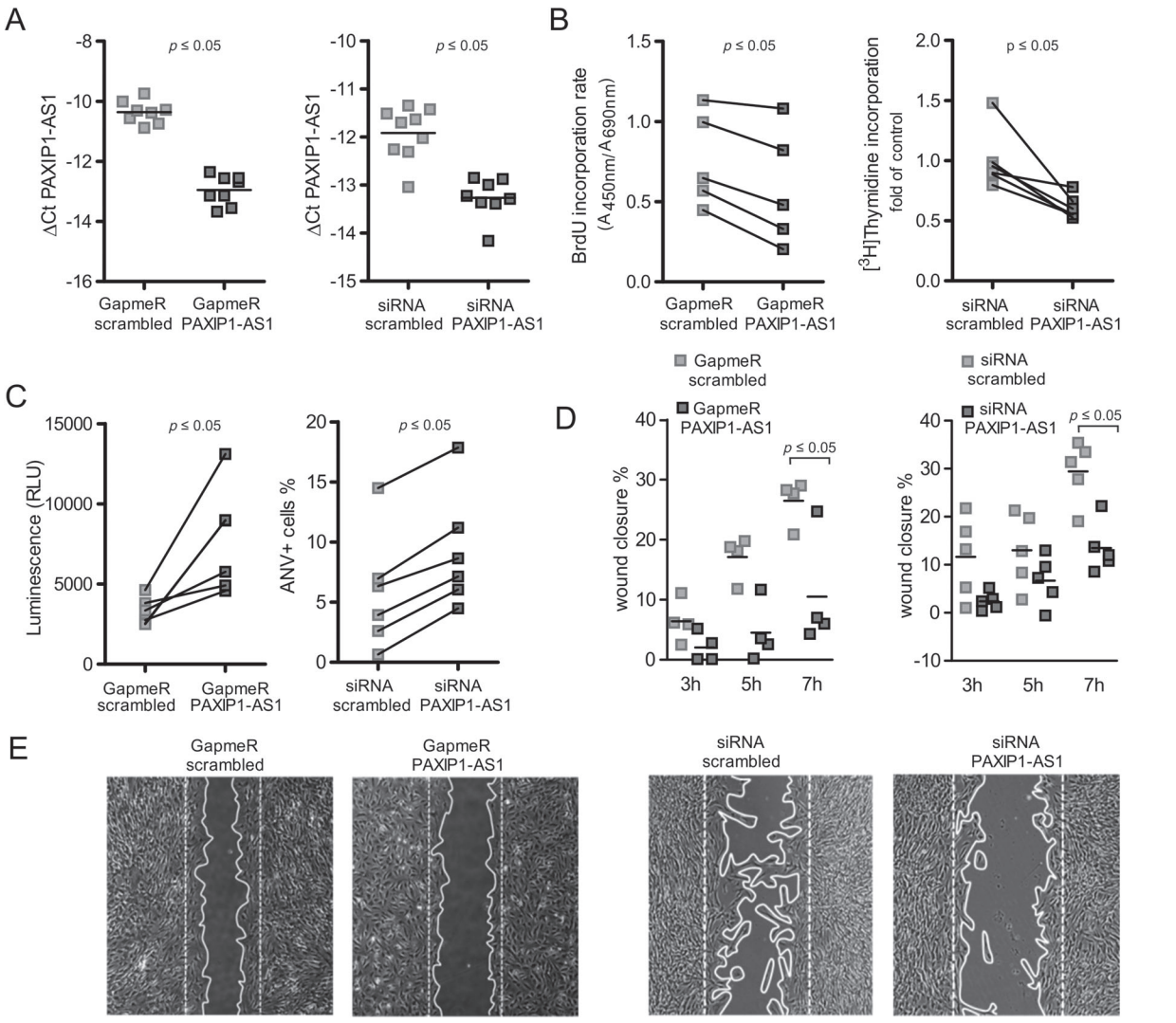

Figure 4. Reduced expression of *PAXIP1-AS1* interferes with proliferative, apoptotic, and migratory properties of PASMCs. (A) Expression levels of *PAXIP1-AS1* after LNA-GapmeR or siRNA-mediated knockdown as determined by qRT-PCR. (B) Proliferation of PASMCs determined by BrdU or [^{3}H]thymidine incorporation, respectively. (C) Apoptosis measurements in PASMCs determined by luminescence-based measurement of active caspase 3/7 and flow cytometric AnV/PI staining, respectively. (D) Quantification of a scratch wound-healing assay to investigate the migratory behaviour of PASMCs at indicated times. (E) Representative pictures ($t = 7$ h of migration) of D. All readouts (A–E) were performed 48 h post-knockdown. $p \leq 0.05$ as determined by Student's *t*-test.

decreased the apoptosis susceptibility in both donor and IPAH PASMCs (Figure 6G,H), suggesting a role in IPAH-related cellular dysfunction (Figure 6I).

Discussion

To date, transcriptomic profiling of IPAH patients either has often lacked compartment-specific analysis or has been limited by the number of patients analysed. Here, we not only describe an IPAH-specific transcriptome in small remodelled arteries in a comparable large cohort of patients, but also address the potential link between dysfunctional lncRNA regulatory mechanisms and the transcriptional changes implicated in vascular remodelling.

In our compartment-specific gene expression analysis, we identified key transcriptional pathways that were perturbed in IPAH; those included metabolic, neuronal, proliferative, and immunological processes. These processes are tightly interconnected. In IPAH, increased proliferation and migration of SMCs can be associated with metabolic changes [37,38]. Adaptions of metabolic processes might be necessary to keep up with the increased energy expenditure or, vice versa, increased energy utilisation might induce a hyperproliferative phenotype. Interestingly, neuronal [39,40] as well as inflammatory mediators [41] can influence a cell's metabolism and growth response, and immunological as well neuronal components have been described in IPAH [42,43]. Given this tight connection of deregulated pathways in remodelled arteries in IPAH, it is apparent that targeting one mechanism might not be sufficient to induce reverse vascular remodelling. In contrast, upstream control mechanisms which simultaneously affect multiple

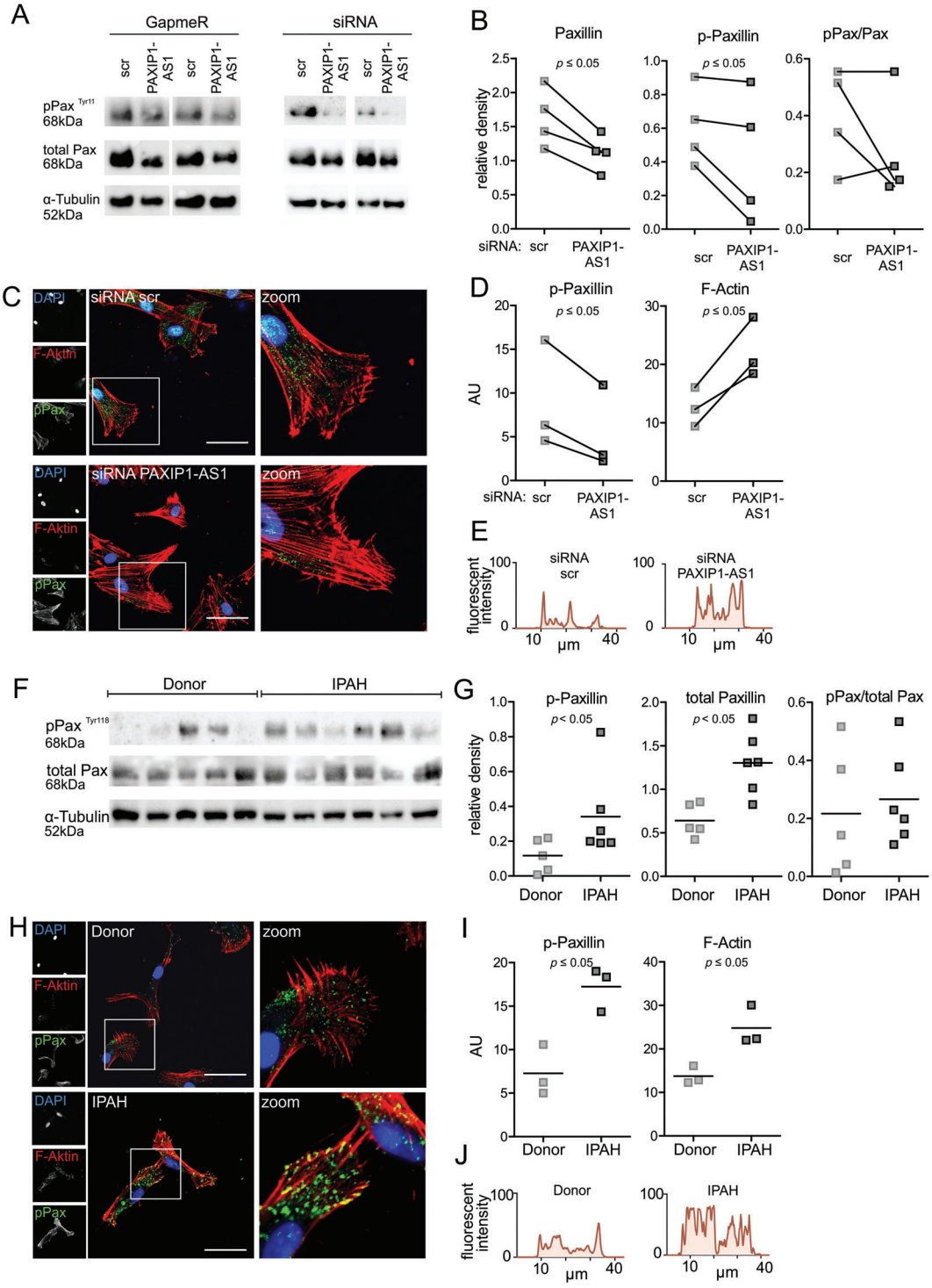

Figure 5. Paxillin is a downstream effector of the lncRNA *PAXIP1-AS1* in donor PASMCs and is increased in PASMCs from IPAH patients. (A) p-Paxillin (Tyr118) and total paxillin expression relative to α-tubulin 48 h after GapmeR- or siRNA-mediated knockdown of *PAXIP1-AS1* in donor PASMCs, as determined by immunoblotting and quantified by densitometry (B). (C) Immunofluorescence of donor PASMCs 48 h after siRNA-mediated *PAXIP1-AS1* knockdown of p-paxillin (green), F-actin (phalloidin, red), and nucleus (DAPI, blue). Scale bar = 50 μm. (D) Quantification of fluorescent intensity of p-paxillin and F-actin. AU = arbitrary units. (E) Representative F-actin cross-sectional fluorescent plots. p-Paxillin (Tyr118) and total paxillin expression relative to α-tubulin in PASMCs from IPAH ($n = 6$) and donor ($n = 5$), as determined by immunoblotting (F) and densitometry (G). (H) Immunofluorescence of PASMCs from IPAH and donor of p-paxillin (green), F-actin (phalloidin, red), and nucleus (DAPI, blue). Scale bar = 50 μm. All immunofluorescence images are representative of three individual experiments with three individual patients and controls, respectively. $p \leq 0.05$ as determined by Student's *t*-test. (I) Quantification of fluorescence intensity of p-paxillin and F-actin. AU = arbitrary units. (J) Representative F-actin cross-sectional fluorescence plots. $p \leq 0.05$ as determined by Student's *t*-test.

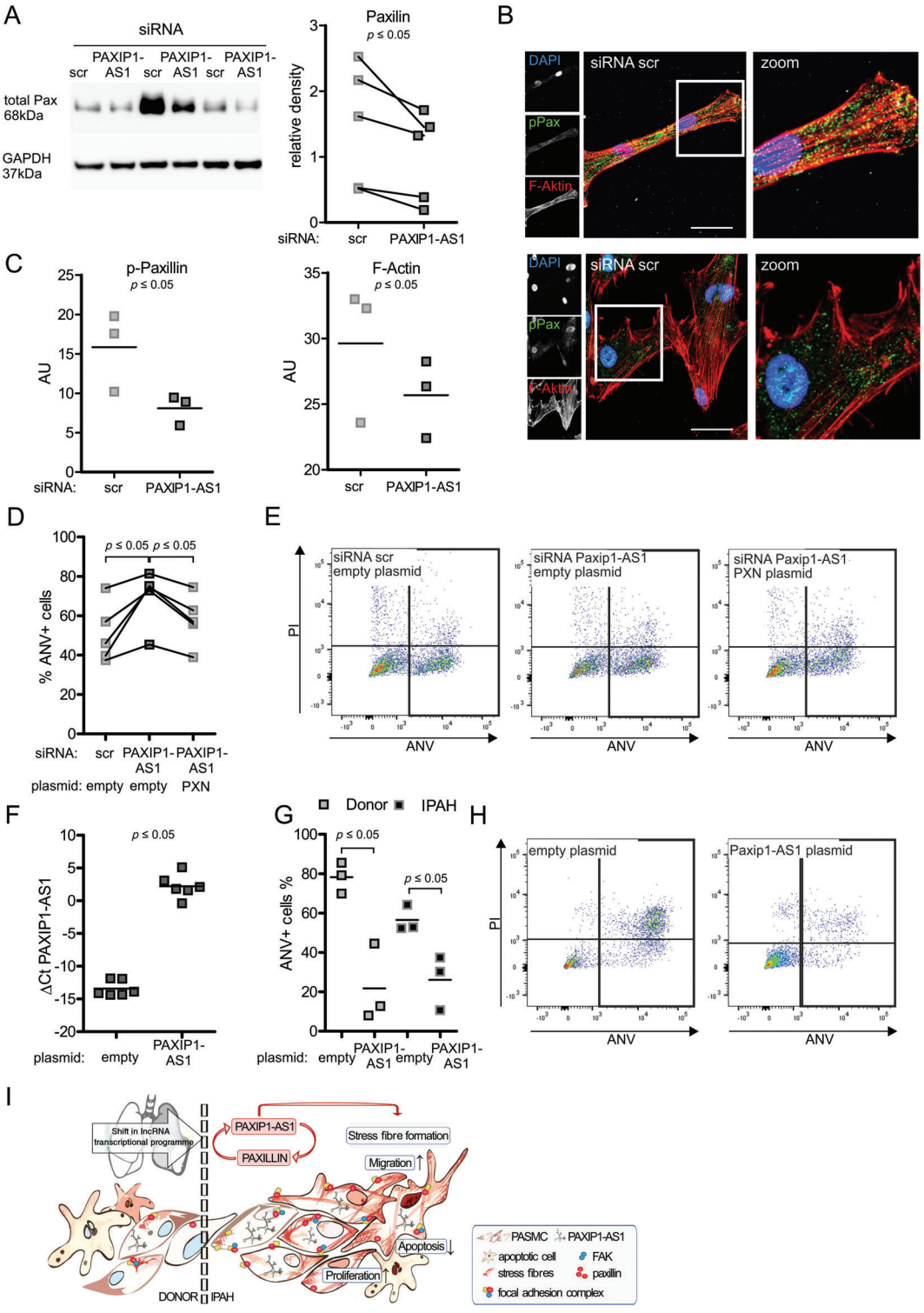

Figure 6. *PAXIP1-AS1* mediates its effect on apoptosis via paxillin in IPAH PASMCs. (A) Total paxillin levels relative to GAPDH 48 h after siRNA-mediated knockdown of *PAXIP1-AS1* in IPAH PASMCs, as determined by immunoblotting and densitometry. $n = 5$. (B) Immunofluorescence of IPAH PASMCs 48 h after siRNA-mediated *PAXIP1-AS1* knockdown of p-paxillin (green), F-actin (phalloidin, red), and nucleus (DAPI, blue). Scale bar = 50 µm. (C) Quantification of fluorescence intensity of p-paxillin and F-actin. AU = arbitrary units. (D) Apoptosis measurements in IPAH PASMCs determined by flow cytometric AnV/PI staining 48 h after siRNA-mediated *PAXIP1-AS1* knockdown and co-transfection with empty or *PXN* overexpression plasmid. (E) Representative flow cytometric scatter plots. (F) Expression levels of *PAXIP1-AS1* 48 h after transfection with *PAXIP1-AS1* overexpression plasmid in donor and IPAH PASMCs. (G) Apoptosis measurements in donor and IPAH PASMCs determined by flow cytometric AnV/PI staining 48 h after transfection with *PAXIP1-AS1* overexpression plasmid. (H) Representative flow cytometric scatter plots. (I) Schematic model of *PAXIP1-AS1* regulation on PASMC function in IPAH. $p \leq 0.05$ as determined by Student's *t*-test, one-way ANOVA followed by Dunnett's multiple comparison test, or two-way ANOVA followed by Bonferroni post-test.

transcriptional pathways might be able to overcome this limitation.

LncRNAs have emerged as critical determinants in human diseases. They can regulate gene expression at epigenetic, transcriptional, and translational levels. Thus, changes in the lncRNA expression profile can be associated with pathological alterations within the coding transcriptome. In this respect, lncRNAs have great capacity for gene regulation [44]. In pulmonary vascular remodelling, little is known about the involvement of lncRNAs in disease development and progression. Only a few recent studies have shown their contribution to vascular smooth muscle cell proliferation or apoptosis (e.g. *MALAT1* [45] or *LnRPT* [46]) and only one study has investigated the lncRNA profile in PAH patients using peripheral blood lymphocytes [47]. Here, we have demonstrated that transcriptional reprogramming in small remodelled arteries (intima and media) is associated with a specific lncRNA expression profile in IPAH. Importantly, the lncRNA transcriptome can be highly cell type and disease-specific [48], and thus can be used to stratify disease subtypes or monitor disease progression.

Among many differentially regulated lncRNAs, we identified *PAXIP1-AS1* as strongly regulated in IPAH small pulmonary arteries, PASMCs, and adventitial fibroblasts. In general, *PAXIP1-AS1* expression was not limited to the lung or any specific cell type, which differs from other reported ncRNAs, e.g. miR206 or miR126 [49–51]. Under physiological conditions, *PAXIP1-AS1* expression is ubiquitous but comparably very low. Its upregulation during disease therefore suggests a crucial role. In that regard, we identified *PAXIP1-AS1* as a critical regulator of PASMC function. The function of a given lncRNA depends on its subcellular localisation and the presence of functional RNA sequences on the transcript. In PASMCs, *PAXIP1-AS1* was ubiquitously localised in the nucleus and in the cytoplasm, and its secondary structure harboured several functional elements. *PAXIP1-AS1* contained several Alu elements in two separate regions. Alu elements belong to the group of short interspersed repeated sequences (SINEs) and are mostly associated with function in the cytoplasm, where they mediate mRNA stability [52]. The *PAXIP1-AS1* transcript also harboured miRNA binding sites. Sponging of miRNAs is another feature that is associated with a cytoplasmic function of lncRNAs. We also identified A- and C-rich tracts on the *PAXIP1-AS1* transcript. These tracts can potentially infer transcriptional regulation, either via epigenetic modulation or via interaction with transcription factors (TFs) [53,54]. Indeed, several binding sites for TFs were revealed on the *PAXIP1-AS1* transcript. The list included some implicated in PH, such as HIF2α, HIF1α, NFAT, NFκB, and FOXO1 [55]. In general, the interaction of an lncRNA with a TF can be multifunctional; it can either inhibit gene expression by acting as a decoy for TF binding or facilitate gene expression by promoting TF accessibility/recruitment to enhancer elements [56]. Taken together, it is apparent that certain structural RNA elements can exert different functional effects depending on the subcellular localisation of the lncRNA. This spatio-temporal action of lncRNAs also applies to *PAXIP1-AS1*. In comparison to PASMCs, where *PAXIP1-AS1* is located both in the cytoplasm and in the nucleus, it was found to be retained in the nucleus in HEK-293 cells [35]. This resulted in functional characteristics differing from our observation, such as opposite proliferative effects.

In PASMCs, *PAXIP1-AS1* knockdown interfered with the PAH-related cellular function by inhibiting migration and proliferation, while increasing apoptotic susceptibility. Accordingly, overexpression of *PAXIP1-AS1* in both donor and IPAH PASMCs led to apoptosis resistance. This suggests that *PAXIP1-AS1* can potentially modulate PASMC-mediated vascular remodelling events. The key pathways that were dependent on *PAXIP1-AS1* and strongly perturbed after knockdown were ECM–receptor interaction and focal adhesions. Both pathways are tightly interconnected, as cell motility depends on a functional interaction of focal adhesions with the surrounding extracellular matrix. Thus, changes in focal adhesions are central to the migratory and proliferative maladaptation of PASMCs in PAH. Indeed, paxillin and other adapter proteins of the focal adhesion complex are strongly associated with IPAH pathology [57–59]. Our transcriptomic analysis and complementary cellular assays identified paxillin as a downstream target of *PAXIP1-AS1*. Knockdown of *PAXIP1-AS1* potently reduced paxillin levels and concomitantly induced a cytoskeletal disruption in donor and IPAH PASMCs, which was accompanied by increased apoptotic susceptibility. Overexpression of *PXN* reversed this effect, and simultaneously increased *PAXIP1-AS1* expression levels (supplementary material, Figure S8A). This suggests a reciprocal dependency of the PAXIP1-AS1–paxillin axis in the mediation of the IPAH phenotype. Interestingly, in addition to paxillin, *PAXIP1-AS1* knockdown also resulted in decreased FAK levels. In IPAH, it has previously been observed that FAK and paxillin levels are co-regulated [59] – a notion substantiated by this study. Together, this suggests that *PAXIP1-AS1* knockdown induced an impairment of the focal adhesion axis, from integrins to actin filaments. While targeting cell motility in vascular remodelling seems promising at first, a loss of function of any member of the focal adhesion complex might be deleterious, due to their involvement in fundamental cellular processes.

In addition to focal adhesion, lncRNA *PAXIP1-AS1* also controlled other critical pathways of PAH pathology. Among the most significantly downregulated pathways after *PAXIP1-AS1* knockdown in PASMCs were also proliferative processes, axon guidance, and sugar metabolism. Interestingly, these pathways mirror the processes that we identified in the compartment-specific transcriptomic analysis of small remodelled arteries. These findings indicate that (1) these processes are

pivotal to the IPAH pathology, (2) IPAH-specific pathological changes are strongly associated with a tightly regulated transcriptional programme, and (3) lncRNAs can act as important regulators in these cellular events in IPAH pathology.

At the moment, it is still unclear whether *PAXIP1-AS1* is causative in disease development or merely a consequence of remodelling processes. Two major limitations of this study in answering this question are (1) its lack of sequence conservation in animals, and (2) the use of human transplanted lungs that always reflect end-stage disease.

Taken together, a multitude of pathways and single molecules finally converge in the manifestation of the maladaptive cellular phenotype in IPAH. The identification of lncRNA *PAXIP1-AS1* as a critical component of the dysfunctional control machinery adds another piece to the complex patho-mechanism of IPAH.

Acknowledgements

GK acknowledges the funding of the Jubilee Foundation of the Austrian National Bank (ÖNB 16187) and Austrian Science Fund (FWF, P27848-B28). HTP was funded by the Austrian Research Promotion Agency (FFG, 858308) and trained within the frame of the PhD programme DK-Molin of the Medical University of Graz. We would like to thank Eva Grasmann and Daniela Rainer (Ludwig Boltzmann Institute for Lung Vascular Research, Graz, Austria) for their excellent technical assistance.

Author contributions statement

KJ, HTP, LMM, MB, and GK conceived the study and drafted the manuscript. KJ, HTP, LMM, JW, and JH carried out experiments and performed data analysis. KS and WK performed data collection. HO and AO contributed to study design and data interpretation.

References

1. Rubin LJ. Primary pulmonary hypertension. *N Engl J Med* 1997; **336:** 111–117.
2. Jones PL, Cowan KN, Rabinovitch M. Tenascin-C, proliferation and subendothelial fibronectin in progressive pulmonary vascular disease. *Am J Pathol* 1997; **150:** 1349–1360.
3. Humbert M, Morrell NW, Archer SL, *et al.* Cellular and molecular pathobiology of pulmonary arterial hypertension. *J Am Coll Cardiol* 2004; **43:** 13S–24S.
4. Morrell NW, Yang X, Upton PD, *et al.* Altered growth responses of pulmonary artery smooth muscle cells from patients with primary pulmonary hypertension to transforming growth factor-beta(1) and bone morphogenetic proteins. *Circulation* 2001; **104:** 790–795.
5. McMurtry MS, Archer SL, Altieri DC, *et al.* Gene therapy targeting survivin selectively induces pulmonary vascular apoptosis and reverses pulmonary arterial hypertension. *J Clin Invest* 2005; **115:** 1479–1491.
6. Archer SL, Gomberg-Maitland M, Maitland ML, *et al.* Mitochondrial metabolism, redox signaling, and fusion: a mitochondria-ROS-HIF-1α-Kv1.5 O2-sensing pathway at the intersection of pulmonary hypertension and cancer. *Am J Physiol Heart Circ Physiol* 2008; **294:** H570–H578.
7. Tuder RM, Davis LA, Graham BB. Targeting energetic metabolism: a new frontier in the pathogenesis and treatment of pulmonary hypertension. *Am J Respir Crit Care Med* 2012; **185:** 260–266.
8. Ma L, Chung WK. The role of genetics in pulmonary arterial hypertension. *J Pathol* 2017; **241:** 273–280.
9. Morrell NW. Pulmonary hypertension due to *BMPR2* mutation: a new paradigm for tissue remodeling? *Proc Am Thorac Soc* 2006; **3:** 680–686.
10. Newman JH, Wheeler L, Lane KB, *et al.* Mutation in the gene for bone morphogenetic protein receptor II as a cause of primary pulmonary hypertension in a large kindred. *N Engl J Med* 2001; **345:** 319–324.
11. Kapranov P, Cheng J, Dike S, *et al.* RNA maps reveal new RNA classes and a possible function for pervasive transcription. *Science* 2007; **316:** 1484–1488.
12. Luco RF. The non-coding genome: a universe in expansion for fine-tuning the coding world. *Genome Biol* 2013; **14:** 314.
13. Guttman M, Rinn JL. Modular regulatory principles of large non-coding RNAs. *Nature* 2012; **482:** 339–346.
14. Brockdorff N. Noncoding RNA and Polycomb recruitment. *RNA* 2013; **19:** 429–442.
15. Joh RI, Palmieri CM, Hill IT, *et al.* Regulation of histone methylation by noncoding RNAs. *Biochim Biophys Acta* 2014; **1839:** 1385–1394.
16. Brunner AL, Beck AH, Edris B, *et al.* Transcriptional profiling of long non-coding RNAs and novel transcribed regions across a diverse panel of archived human cancers. *Genome Biol* 2012; **13:** R75.
17. Morris KV, Mattick JS. The rise of regulatory RNA. *Nat Rev Genet* 2014; **15:** 423–437.
18. Carninci P, Kasukawa T, Katayama S, *et al.* The transcriptional landscape of the mammalian genome. *Science* 2005; **309:** 1559–1563.
19. Iyer MK, Niknafs YS, Malik R, *et al.* The landscape of long noncoding RNAs in the human transcriptome. *Nat Genet* 2015; **47:** 199–208.
20. Brock M, Haider TJ, Vogel J, *et al.* The hypoxia-induced microRNA-130a controls pulmonary smooth muscle cell proliferation by directly targeting CDKN1A. *Int J Biochem Cell Biol* 2015; **61:** 129–137.
21. Brock M, Samillan VJ, Trenkmann M, *et al.* AntagomiR directed against miR-20a restores functional BMPR2 signalling and prevents vascular remodelling in hypoxia-induced pulmonary hypertension. *Eur Heart J* 2014; **35:** 3203–3211.
22. Courboulin A, Paulin R, Giguere NJ, *et al.* Role for miR-204 in human pulmonary arterial hypertension. *J Exp Med* 2011; **208:** 535–548.
23. Deng L, Blanco FJ, Stevens H, *et al.* MicroRNA-143 activation regulates smooth muscle and endothelial cell crosstalk in pulmonary arterial hypertension. *Circ Res* 2015; **117:** 870–883.
24. Kim J, Kang Y, Kojima Y, *et al.* An endothelial apelin-FGF link mediated by miR-424 and miR-503 is disrupted in pulmonary arterial hypertension. *Nat Med* 2013; **19:** 74–82.
25. Chang TH, Huang HY, Hsu JB, *et al.* An enhanced computational platform for investigating the roles of regulatory RNA and for identifying functional RNA motifs. *BMC Bioinformatics* 2013; **14**(suppl 2): S4.
26. Kong L, Zhang Y, Ye ZQ, *et al.* CPC: assess the protein-coding potential of transcripts using sequence features and support vector machine. *Nucleic Acids Res* 2007; **35:** W345–W349.

27. Wang L, Park HJ, Dasari S, *et al.* CPAT: Coding-Potential Assessment Tool using an alignment-free logistic regression model. *Nucleic Acids Res* 2013; **41:** e74.
28. Gruber AR, Lorenz R, Bernhart SH, *et al.* The Vienna RNA websuite. *Nucleic Acids Res* 2008; **36:** W70–W74.
29. Altschul SF, Gish W, Miller W, *et al.* Basic local alignment search tool. *J Mol Biol* 1990; **215:** 403–410.
30. Morgulis A, Coulouris G, Raytselis Y, *et al.* Database indexing for production MegaBLAST searches. *Bioinformatics* 2008; **24:** 1757–1764.
31. NCBI Resource Coordinators. Database resources of the National Center for Biotechnology Information. *Nucleic Acids Res* 2016; **44:** D7–D19.
32. Xia J, Gill EE, Hancock RE. NetworkAnalyst for statistical, visual and network-based meta-analysis of gene expression data. *Nat Protoc* 2015; **10:** 823–844.
33. Gagnon KT, Li L, Janowski BA, *et al.* Analysis of nuclear RNA interference in human cells by subcellular fractionation and Argonaute loading. *Nat Protoc* 2014; **9:** 2045–2060.
34. Hoffmann J, Marsh LM, Pieper M, *et al.* Compartment-specific expression of collagens and their processing enzymes in intrapulmonary arteries of IPAH patients. *Am J Physiol Lung Cell Mol Physiol* 2015; **308:** L1002–L1013.
35. Weirick T, Militello G, Ponomareva Y, *et al.* Logic programming to infer complex RNA expression patterns from RNA-seq data. *Brief Bioinform* 2018; **19:** 199–209.
36. Johnsson P, Lipovich L, Grander D, *et al.* Evolutionary conservation of long non-coding RNAs; sequence, structure, function. *Biochim Biophys Acta* 2014; **1840:** 1063–1071.
37. Barnes JW, Tian L, Heresi GA, *et al.* O-linked β-N-acetylglucosamine transferase directs cell proliferation in idiopathic pulmonary arterial hypertension. *Circulation* 2015; **131:** 1260–1268.
38. Zhang S, Fantozzi I, Tigno DD, *et al.* Bone morphogenetic proteins induce apoptosis in human pulmonary vascular smooth muscle cells. *Am J Physiol Lung Cell Mol Physiol* 2003; **285:** L740–L754.
39. Freund-Michel V, Cardoso Dos Santos M, Guignabert C, *et al.* Role of nerve growth factor in development and persistence of experimental pulmonary hypertension. *Am J Respir Crit Care Med* 2015; **192:** 342–355.
40. Kwapiszewska G, Chwalek K, Marsh LM, *et al.* BDNF/TrkB signaling augments smooth muscle cell proliferation in pulmonary hypertension. *Am J Pathol* 2012; **181:** 2018–2029.
41. Hurst LA, Dunmore BJ, Long L, *et al.* TNFα drives pulmonary arterial hypertension by suppressing the BMP type-II receptor and altering NOTCH signalling. *Nat Commun* 2017; **8:** 14079.
42. Marsh LM, Jandl K, Grunig G, *et al.* The inflammatory cell landscape in the lungs of patients with idiopathic pulmonary arterial hypertension. *Eur Respir J* 2018; **51:** pii: 1701214.
43. Crnkovic S, Egemnazarov B, Jain P, *et al.* NPY/Y(1) receptor-mediated vasoconstrictory and proliferative effects in pulmonary hypertension. *Br J Pharmacol* 2014; **171:** 3895–3907.
44. Cao J. The functional role of long non-coding RNAs and epigenetics. *Biol Proced Online* 2014; **16:** 11.
45. Brock M, Schuoler C, Leuenberger C, *et al.* Analysis of hypoxia-induced noncoding RNAs reveals metastasis-associated lung adenocarcinoma transcript 1 as an important regulator of vascular smooth muscle cell proliferation. *Exp Biol Med* 2017; **242:** 487–496.
46. Chen J, Guo J, Cui X, *et al.* The long non-coding RNA LnRPT is regulated by PDGF-BB and modulates proliferation of pulmonary artery smooth muscle cells. *Am J Respir Cell Mol Biol* 2018; **58:** 181–193.
47. Han B, Bu P, Meng X, *et al.* Microarray profiling of long non-coding RNAs associated with idiopathic pulmonary arterial hypertension. *Exp Ther Med* 2017; **13:** 2657–2666.
48. Liu SJ, Horlbeck MA, Cho SW, *et al.* CRISPRi-based genome-scale identification of functional long noncoding RNA loci in human cells. *Science* 2017; **355:** pii: aah7111.
49. Paulin R, Sutendra G, Gurtu V, *et al.* A miR-208–Mef2 axis drives the decompensation of right ventricular function in pulmonary hypertension. *Circ Res* 2015; **116:** 56–69.
50. Potus F, Malenfant S, Graydon C, *et al.* Impaired angiogenesis and peripheral muscle microcirculation loss contribute to exercise intolerance in pulmonary arterial hypertension. *Am J Respir Crit Care Med* 2014; **190:** 318–328.
51. Potus F, Ruffenach G, Dahou A, *et al.* Downregulation of microRNA-126 contributes to the failing right ventricle in pulmonary arterial hypertension. *Circulation* 2015; **132:** 932–943.
52. Rashid F, Shah A, Shan G. Long non-coding RNAs in the cytoplasm. *Genomics Proteomics Bioinformatics* 2016; **14:** 73–80.
53. Gupta RA, Shah N, Wang KC, *et al.* Long non-coding RNA HOTAIR reprograms chromatin state to promote cancer metastasis. *Nature* 2010; **464:** 1071–1076.
54. Hung T, Wang Y, Lin MF, *et al.* Extensive and coordinated transcription of noncoding RNAs within cell-cycle promoters. *Nat Genet* 2011; **43:** 621–629.
55. Pullamsetti SS, Perros F, Chelladurai P, *et al.* Transcription factors, transcriptional coregulators, and epigenetic modulation in the control of pulmonary vascular cell phenotype: therapeutic implications for pulmonary hypertension (2015 Grover Conference series). *Pulm Circ* 2016; **6:** 448–464.
56. Ferre F, Colantoni A, Helmer-Citterich M. Revealing protein–lncRNA interaction. *Brief Bioinform* 2016; **17:** 106–116.
57. Veith C, Marsh LM, Wygrecka M, *et al.* Paxillin regulates pulmonary arterial smooth muscle cell function in pulmonary hypertension. *Am J Pathol* 2012; **181:** 1621–1633.
58. Veith C, Zakrzewicz D, Dahal BK, *et al.* Hypoxia- or PDGF-BB-dependent paxillin tyrosine phosphorylation in pulmonary hypertension is reversed by HIF-1α depletion or imatinib treatment. *Thromb Haemost* 2014; **112:** 1288–1303.
59. Paulin R, Meloche J, Courboulin A, *et al.* Targeting cell motility in pulmonary arterial hypertension. *Eur Respir J* 2014; **43:** 531–544.
*60. Hoffmann J, Wilhelm J, Marsh LM, *et al.* Distinct differences in gene expression patterns in pulmonary arteries of patients with chronic obstructive pulmonary disease and idiopathic pulmonary fibrosis with pulmonary hypertension. *Am J Respir Crit Care Med* 2014; **190:** 98–111.
*61. Ritchie ME, Phipson B, Wu D, *et al.* limma powers differential expression analyses for RNA-sequencing and microarray studies. *Nucleic Acids Res* 2015; **43:** e47.
*62. Gentleman RC, Carey VJ, Bates DM, *et al.* Bioconductor: open software development for computational biology and bioinformatics. *Genome Biol* 2004; **5:** R80.
*63. Smyth GK, Speed T. Normalization of cDNA microarray data. *Methods* 2003; **31:** 265–273.
*64. Shannon P, Markiel A, Ozier O, *et al.* Cytoscape: a software environment for integrated models of biomolecular interaction networks. *Genome Res* 2003; **13**: 2498–2504.
*65. Wei S, Gao X, Du J, *et al.* Angiogenin enhances cell migration by regulating stress fiber assembly and focal adhesion dynamics. *PLoS One* 2011; **6**: e28797.
*66. Schmittgen TD, Livak KJ. Analyzing real-time PCR data by the comparative C_T method. *Nat Protoc* 2008; **3**: 1101–1108.

*Cited only in supplementary material.

SUPPLEMENTARY MATERIAL ONLINE

Supplementary materials and methods

Supplementary figure legends

Figure S1. Enriched KEGG pathways in LCM array

Figure S2. *PAXIP1-AS1* expression in various tissues

Figure S3. Coding potential assessment

Figure S4. *PAXIP1-AS1 in situ* hybridisation

Figure S5. *PAXIP1-AS1* after cytokine stimulation

Figure S6. Cross-sectional F-actin plots

Figure S7. *PAXIP1-AS1* influences FAK expression

Figure S8. *PAXIP1-AS1* and PXN expression

Table S1. Differentially regulated coding genes in IPAH

Table S2. Differentially regulated non-coding genes in IPAH

Table S3. Functional regions in *PAXIP1-AS1*

Table S4. Transcription factor binding sites in the *PAXIP1-AS1* transcript

Table S5. miRNA target sites in the *PAXIP1-AS1* transcript

Table S6. *PAXIP1-AS1* knockdown: differentially regulated genes

Table S7. *PAXIP1-AS1* knockdown: list of genes from the top regulated pathways

Table S8. Comparative transcriptomic analysis: differentially regulated genes

Table S9. Primer sequences (mentioned in the supplementary material, Supplementary materials and methods)